Magnetic Resonance in Medicine 51:1153–1162 (2004)

In Vivo Monitoring of Tissue Pharmacokinetics of Liposome/Drug Using MRI: Illustration of Targeted Delivery

Benjamin L. Viglianti,[1] Sheela A. Abraham,[2,3] Charles R. Michelich,[1] Pavel S. Yarmolenko,[4] James R. MacFall,[5] Marcel B. Bally,[2,3] and Mark W. Dewhirst[1,4*]

The purpose of this study was to determine if $MnSO_4$/doxorubicin (DOX) loaded liposomes could be used for in vivo monitoring of liposome concentration distribution and drug release using MRI. In vitro results show that T_1 shortening correlates with $MnSO_4$ concentration. Using a temperature-sensitive liposome formulation, it was found that $MnSO_4$ release significantly shortened T_1. This feature, therefore, suggests that content release can also be measured with these $MnSO_4$-loaded liposomes. The feasibility of monitoring this drug delivery and release-imaging agent was shown in a murine tumor model. Upon tumor heating, nonthermally sensitive liposomes selectively but heterogeneously accumulated in the tumor region. The thermally sensitive liposomes showed a clear pattern of accumulation at the periphery of the tumor, concordant with the release temperature of this formulation (39–40°C). This liposome contrast agent has potential for use with hyperthermia by providing individualized monitoring of tissue drug concentration distribution during or after treatment. This would allow for: 1) modification of treatment variables to improve the uniformity of drug delivery, and 2) provide a means to select patients most likely to benefit from this liposomal drug treatment. Additionally, the drug-loading method used for this liposome is applicable to a wide range of drugs, thereby broadening its applicability. The method is also applicable to other liposomal formulations with triggered release mechanisms. Magn Reson Med 51: 1153–1162, 2004. © 2004 Wiley-Liss, Inc.

Key words: hyperthermia; chemotherapy; pharmacokinetics; liposomes

Effective cancer chemotherapy depends on delivery of drugs to cells at cytotoxic concentrations. Due to inherent perfusion limitations in tumors, delivery of drugs may be hindered (1). However, aside from using radiolabeled drugs and nuclear medicine scans (2), methods to measure drug concentration distributions noninvasively and at therapeutic concentrations have not been reported. In this article we present an approach that can monitor liposomal drug concentration distributions as well as drug release by using a novel $MnSO_4$-doxorubicin (DOX) formulation. Doxorubicin is classified as a cytotoxic anthracycline antibiotic isolated from cultures of *Streptomyces peucetius* var. *caesius*. It consists of a naphthacenequinone nucleus linked through a glycosidic bond and amino sugar (daunosamine). The molecule is amphoteric, containing acidic functions in the ring phenolic groups and a basic function in the sugar amino group. It binds to nucleic acids, presumably by specific intercalation of the planar anthracycline nucleus with the DNA double helix. It has also been shown to bind with cell membranes as well as plasma proteins (3).

We show that this liposome can be used to monitor drug delivery and liposomal release in a murine flank tumor model. The liposomes can be visualized outside the reticulo-endothelial system (RES), thereby making this approach practical for imaging outside the liver and spleen. The basis for imaging is the presence of $MnSO_4$ in the interior of the liposomes, which is used to load DOX (4). This method of loading uses the metal concentration gradient (4). It is believed that two DOX molecules are coordinated to each Mn^{2+} atom within the liposome (4).

The relaxivity of Mn is similar to that of Gd, thereby making this liposome potentially suitable as a contrast agent (5–7). Other approaches have been used to image liposomes (8,9), but none have used a liposome that is a dual drug delivery and imaging vehicle. Prior MRI-based reports have focused on obtaining images in the RES (9–14), which tends to concentrate liposomes following intravenous administration. When metal ions are retained inside liposomes, MR signal intensity is relatively unaffected (13,15). Shortening of T_1, for example, depends on interaction between metal ions and water (16). Because water cannot easily cross the lipid membrane except with specialized lipid formulations designed to be relatively unstable (15,16), signal intensity changes are low (13). An alternative has been to attach paramagnetic metals to the outer liposome surface (13,15). These surface attached contrast agents have shown T_1 shortening essentially equivalent to that of free ions.

Prior studies have shown that hyperthermia (HT) (40–42°C) can increase liposomal uptake in tumors (1,17–19). Thus, to demonstrate that liposome accumulation and drug release can be observed, we compared the MR signal intensity of $MnSO_4$-DOX loaded into two types of liposomes under in vitro and in vivo conditions, with and without heating: 1) a nonthermally sensitive formulation

[1]Department of Biomedical Engineering, Duke University, Durham, North Carolina.

[2]Advanced Therapeutics-Medical Oncology, BC Cancer Agency, Vancouver, Canada.

[3]Department of Pathology and Laboratory Medicine, University of British Columbia, Vancouver, Canada.

[4]Department of Radiation Oncology, Duke University Medical Center, Durham, North Carolina.

[5]Department of Radiology, Duke University Medical Center, Durham, North Carolina.

Grant sponsor: DOD Breast Cancer Research Program; Grant number: DAMD17-03-1-0348; Grant sponsor: NIH/NCI Grant numbers: CA42745; NIH/NCRR P4105959; NIH/NCI R24 CA092656.

*Correspondence to: Mark W. Dewhirst, Dept. of Radiation Oncology, Duke University Medical Center, 201 MSRB Box 3455, Research Drive, Durham, NC 27705. E-mail: dewhirst@radonc.duke.edu

Received 29 April 2003; revised 5 January 2004; accepted 7 January 2004.

DOI 10.1002/mrm.20074

Published online in Wiley InterScience (www.interscience.wiley.com).

(NTSL), and 2) a low-temperature sensitive liposome (LTSL) formulation that releases contents within seconds of reaching its transition temperature (39.5–40°C) (20).

MATERIALS AND METHODS

Liposome Materials

Doxorubicin hydrochloride (DOX) (Faulding Quebec, Canada) was purchased from the British Columbia Cancer Agency. 1,2 Distearoyl-sn-glycero-3-phosphocholine (DSPC), 1,2 dipalmitoyl-sn-glycerol-3-phosphocholine (DPPC), 1-stearoyl-2-hydroxy-sn-glycero-3-phosphocholine (MSPC), and 1,2 distearoyl-sn-glycero-3-phosphoethanolamine-N-(21) were obtained from Avanti Polar Lipids (Alabaster, AL). Cholesterol (Chol), Sephadex G-50, and all other chemicals were obtained from the Sigma Chemical Co. (St. Louis, MO).

Preparation of Liposomes

Liposomes were made from either DSPC/Chol (55:45) (mol/mol), DPPC-DSPE-PEG_{2000} (95:5) (mol:mol), DPPC-MSPC-DSPE-PEG_{2000} (90:10:4) (mol:mol) and were prepared by the extrusion methods. Lipids, at the indicated ratios, were dissolved in a chloroform-methanol mixture. Solvent was removed under a gentle stream of nitrogen gas followed by placement under a high vacuum for at least 4 hr to remove residual solvent. Dried samples were hydrated (such that the final lipid concentration was ~100 mg/mL) with 300 mM $MnSO_4$ adjusted to pH 3.5 by addition of hydrochloric acid. Lipid hydration was performed at 55°C for ~30 min. The multilamellar vesicles were extruded 10 times through stacked polycarbonate filters of 0.1 and 0.08 μm pore size at 55°C using a water-jacketed Extruder (Northern Lipids, Vancouver, Canada) (4). The mean size distribution of all liposome preparations was determined using a Nicomp Submicron Particle Sizer Model 270 (Pacific Scientific, Santa Barbara, CA) operating at 632.8 nm and was determined to have average size diameter of 100–120 nm (22). Phospholipid was quantitated using the Fiske and Subbarow phosphate assay (23). Briefly, 700 μL of 70% perchloric acid was added to lipid samples and heated to 180–200°C for 2 hr until samples were colorless. Samples were cooled and 700 μL of Fiske reagent and 7 mL of ammonium molybdate were added. Samples were subsequently reheated to 100°C for 20 min. Samples were cooled to room temperature and absorbance was read at 820 nm.

Preparation of Ion Gradients for Doxorubicin Encapsulation

Large unilamellar liposomes in the indicated buffers were fractionated on Sephadex G-50 columns (1 mL samples were placed on columns with at least a 20 mL column bed) equilibrated with 300 mM Sucrose/20 mM HEPES (N-(23) piperazine-N′-[2-ethanesulfonic acid]) buffer at pH 7.5. The manganese sulfate procedure for doxorubicin loading was modified from Abraham et al. (4). Following formation of the salt gradient as described above, liposome lipid concentration was adjusted to 10 mg/mL and DOX was added to achieve a drug-to-lipid ratio (wt:wt) of 0.05:1 at 37°C. It is likely that Mn^{2+} is coordinated to the oxygens associated with the C5, C6, and C11 and C12 positions of the DOX molecule. Qualitatively, accumulation of DOX into the liposomes can be observed by a color change from orange-red (free DOX) to dark royal purple for complexed DOX (peak absorbance changes from 550 nm to 480 nm) (4). The accumulation of DOX into liposomes was determined by removing 100 μl aliquots and separating unencapsulated from encapsulated drug on 1 mL Sephadex G-50 (medium) spin columns equilibrated with the appropriate buffer. The concentration of DOX in the excluded fraction was determined by measuring absorbance (at 480 nm) of a solution containing the sample, adjusted to 100 μl with SHE, to which 900 μl of 1% Triton X-100 was added. Prior to assessing absorbance at 480 nm, the sample was placed in a >90°C water-bath until the cloud point of the detergent was observed. Liposome lipid concentrations were determined by using the phosphate assay as described above.

Sample Solution Formation

Liposomes had their concentration converted to an equivalent $MnSO_4$ molarity using the molecular weight of the lipid and an assumption of a 1.2 $\mu l/mmol_{lipid}$ encapsulation volume commonly used to characterize liposome volume from concentration (22). Consequently, a 1-mg/ml lipid concentration with 300 mM $MnSO_4$ encapsulated yielded an $MnSO_4$ solution concentration of 0.437 mM for DPPC-MSPC-DSPE-PEG_{2000} and 0.592 mM for DSPC/Chol assuming full liposome content release occurred. All experiments were standardized to the equivalent $MnSO_4$ concentration assuming complete content release occurred.

Manganese Sulfate Control Stock Solutions

Three control stock solutions of manganese sulfate ($MnSO_4*H_2O$), free DOX, and $MnSO_4*H_2O$ in a molar ratio of 0.902:1 (DOX:Mn), and $MnSO_4*H_2O$ combined with empty thermally sensitive liposomes were used to simulate conditions when the contents had been released. These solutions, along with intact nonthermally sensitive and thermally sensitive liposome solutions containing $MnSO_4$/DOX, were then diluted to concentrations from 0.25–8 mM. The solutions were placed in 5 ml NMR tubes cut to a three-inch length.

In Vitro MRI Scans

All MRI experiments were performed at the Center for In Vivo Microscopy at Duke University in a 2 T 30-cm bore diameter magnet (Signa, GE Medical Systems, Milwaukee, WI). Temperature control in the bore was achieved with an automatic feedback control unit that was initially designed for maintaining temperature of laboratory animals (24). Each experiment had six to eight sample tubes, contained within an exposed sample holder, and placed inside a 3.81-cm birdcage coil. Temperatures on the heating apparatus were chosen at random, the temperature controller was set for each, and bore equilibration occurred within 10 min. A series of T_1-weighted images was then taken in the axial plane with a field of view of 5 cm at an echo time

of 8 ms and TR of 20, 33.3, 66.6, 150, 316, 633, and 1266 ms. Between six and eight temperature points were measured. Each experiment was repeated three times with independently formulated reagents. Liposomes were tested sequentially with a minimum of two measurements below-above and back below the transition temperature for the LTSL (39.5–40°C). The NTSLs were tested in the same manner. If hysteresis were observed this would indicate that the contents had been released.

In Vivo Experiments

Animal Model

A transplantable rat fibrosarcoma (FSA) tumor line used for this study was originally developed by subcutaneous injection of the carcinogen, methylcholanthrene, into Fischer 344 rats (25). The tumor line does not grow in vitro, so it is maintained by serial transplantation. Tumors were allowed to grow to 17–19 mm diameter before use. Animals were kept in standard housing with regular light and dark cycles. They were provided with access to water and food ad libitum. All procedures were approved by the Duke University Animal Care and Use Committee.

Heating Method and Determination of Temperature Distribution

Rats were anesthetized with pentobarbital (Nembutal, 50 mg/kg, IP) and a 16 G catheter was placed through the center of the tumor. The core temperature of the rats was maintained with a rectal temperature-regulated heating pad. Heated water (50 ± 0.1°C, 1.8 ml/s) was passed through the catheter to heat the surrounding tissue. The surface temperature of the catheter was 6°C cooler than the temperature of the heated water. Temperature profiles were measured with a k-type 33.5-gauge hypodermic thermocouple (Omega Probes) in four rats with tumors of 17–19 mm diameter after tumors reached steady state temperature (20–30 min). Measurements were located in three orthogonal planes to the heating catheter; one in the central plane and the other two ±2 mm from the center. Each plane had four measurement tracks taken ±2 and 4 mm from the centerline of the tumor defined by the catheter. The thermocouple was inserted to a depth of 13 mm and retracted every 1 mm, yielding 4 × 13 measurements per plane. The tracks were taken in random order; the measurements within each plane were averaged and converted to a radial distance from the catheter. This yielded 26 radial measurements from 2–9 mm for each plane. The results for each were then fitted to the radial 1D steady state heat transfer equation using Gauss-Newton nonlinear regression implemented on MATLAB (MathWorks, Natick, MA).

The heating profile in the MR unit was measured in three rats. Five thermometer locations were monitored (excluding the rectal thermometer used for core temperature regulation): 1) the air stream; 2) intradermal, perpendicular to the air stream direction; 3) the tumor at the catheter surface; 4) 2.5 mm away from the catheter; and 5) at the base of the tumor adjacent to underlying muscle. The results were also fitted to the radial 1D SS heat transfer equation, as described above, but using a different set of boundary conditions, as described in the Results.

MRI Scan Protocol

Rats were anesthetized with an IP injection of sodium methohexital (Brevital) 45 mg/kg. Atropine sulfate was given IP (0.35 mg/kg) to prevent mucous secretion in the airways. An endotracheal tube (16–18 gauge intracath) was inserted and the rats were mechanically ventilated with isoflurane (1–3%). ECG electrodes were placed on the footpads and a rectal thermistor was used to monitor body temperature and control the feedback-heating device (24). A catheter was placed through the center of the tumor and heated water was passed through it to provide heating, as described above. Tumors were heated for 15–20 min to reach thermal steady state before liposome injection. The rats were administered an IV dose of 200 mg/ml liposomes loaded with 0.05:1 DOX/liposome (wt:wt) yielding 10 mg/kg of DOX.

During MRI scans, heating water was doped with 0.25 M $MnSO_4$ to prevent flow image artifacts through T_2 shortening (5,7). Spoiled gradient recalled echo acquisition was used with a TR of 23 ms, echo time of 1.4 ms, and flip angles of 2, 5, 8, 10, 12, 33, 46, and 60° for the initial T_1-weighted image. Subsequent drug uptake scans were performed at a 33° flip angle. 3D volume images, 16 slices (12 useable) 1.3 mm thick, were taken with a 6 cm field of view yielding an in-plane pixel size of 234 × 234 μm. 1NEX (single image) was used for the first 20 min and 4NEX (four image averaging) was used for the remainder of the experiment for improved signal-to-noise. The numbers of subjects imaged were: 1) LTSL + HT (n = 3); 2) LTSL alone (n = 3), 3) NTSL + HT (n = 3), and 4) NTSL alone (n = 2)

Image Analysis

The MATLAB (MathWorks) software program was used for all image analysis.

In Vitro Experiments Image Analysis

Images were analyzed by selecting a region of interest in the center of each sample tube and measuring average signal intensity. Intensity data were fit using nonlinear least-squares data fitting governed by the Gauss-Newton method, to obtain a T_1 for each concentration tested. Reciprocal T_1 data were plotted as a function of concentration and fitted to a linear regression, yielding relaxivity $(mM*sec)^{-1}$ as the slope. Relaxivity was plotted as a function of temperature.

Image Analysis Methods for In Vivo Studies

Signal Intensity Ratio

In vivo signal intensity ratio (SIR) analysis for LTSL ± HT was done by selecting regions of interest (ROIs) (tumor enhancing, tumor nonenhancing, or muscle region) in each particular slice (26). The mean signal intensities of ROIs at each time point were calculated as the average over all slices within the experiment. Signal intensity of each ROI was normalized at each time point to the average

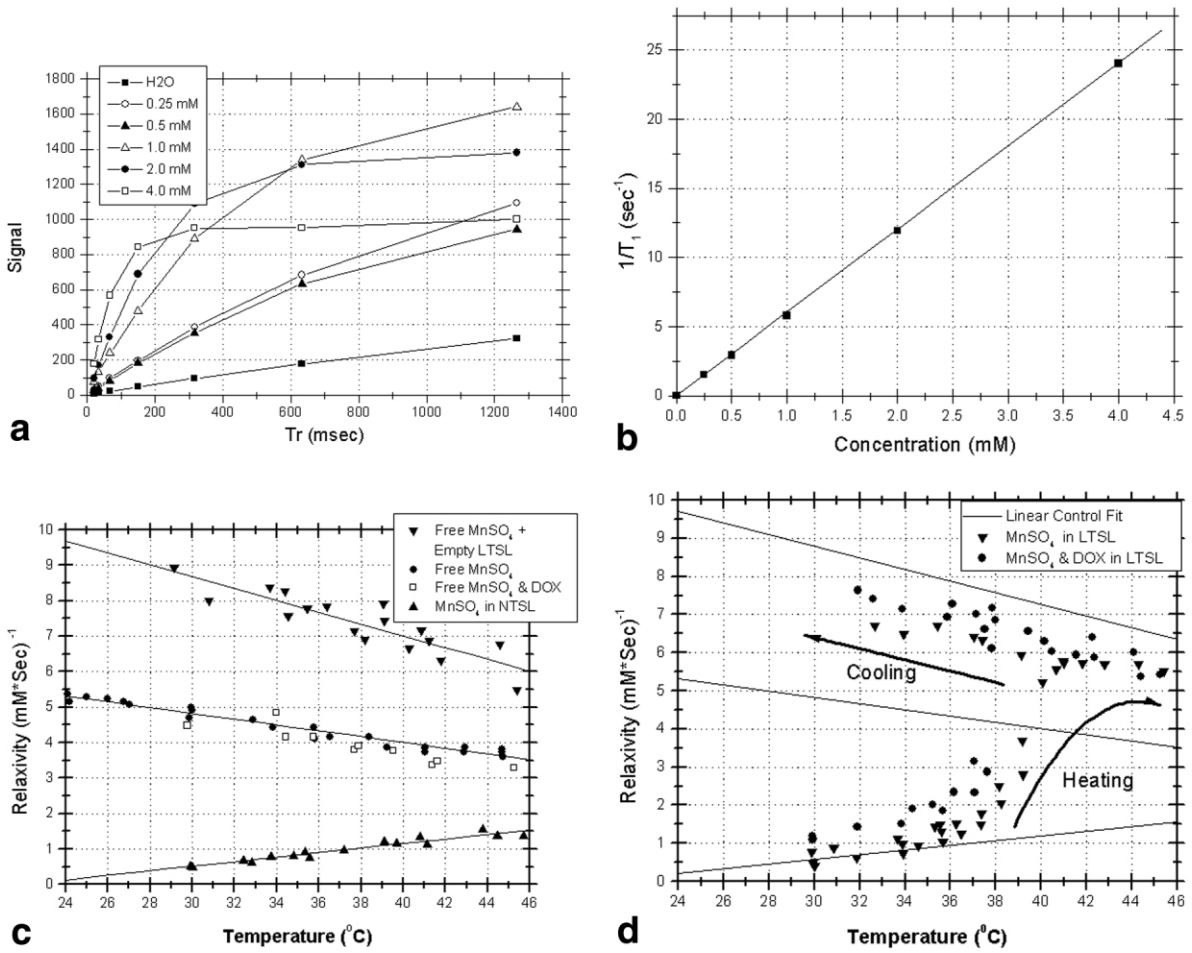

FIG. 1. Baseline relaxivity measurements made at 25°C. Samples were then heated and subsequently cooled to illuminate hysteresis in relaxivity measurements. **a:** Signal intensity vs. repetitions time (msec) between RF excitation pulses at 29.9°C for (■) water, (○) 0.25 mM, (▲) 0.5 mM, (△) 1.0 mM, (●) 2.0 mM, and (□) 4.0 mM $MnSO_4$ + DOX. **b:** $1/T_1$ (sec^{-1}) (as derived from **a**) vs. $MnSO_4$ concentration (mM) at 29.9°C. Slope of this regression is termed relaxivity and represents the change in $1/T_1$ as a function of $MnSO_4$ concentration. **c:** Relaxivity $(mM*sec)^{-1}$ vs. temperature (°C) is shown for (▼) free $MnSO_4$ + empty LTSL, (●) $MnSO_4$, (□) free $MnSO_4$ + DOX, and (▲) $MnSO_4$ in NTSL. Relaxivity decreased linearly with increasing temperature for free $MnSO_4$ but increases with increasing temperature for encapsulated $MnSO_4$. **d:** Relaxivity $(mM*sec)^{-1}$ vs. temperature (°C) is shown for (▼) $MnSO_4$ in LTSL and (●) $MnSO_4$ +DOX in LTSL. Linear regressions from **c** are also shown. LTSL ± DOX relaxivity follows the trend of NTSL encapsulated $MnSO_4$, until the transition temperature is reached. When the transition temperature is reached (39–40°C) rapid increase in relaxivity occurs as $MnSO_4$ is released. With additional heating and subsequent cooling the LTSL ± DOX behaves like $MnSO_4$ + LTSL from **c**.

signal intensity of the muscle ROI yielding the SIR for that particular animal and region. This normalization method was chosen because LTSL and NTSL do not extravasate in muscle, and therefore serves as an internal control (17,19). The SIR for each tumor region was then averaged across animals in each group. The resulting mean values (±SEM) were plotted as a function of time. A tumor nonenhancing region was not present in the LTSL alone group because this showed uniform enhancement

Radial Signal Distribution

Radial analysis of the MR data (RSD) facilitated comparison with the radially symmetric temperature distribution. RSD was performed by calculating the mean and standard error of the mean of the signal intensity for each pixel as a function of radial distance from the center axis of the heating catheter. The data are reported as the mean and standard error of the mean of the signal intensity of pixels with like radial distances. The analysis was performed separately for each slice and time point.

RESULTS

In Vitro Experiments

In vitro experiments were performed to determine the concentration- and temperature-dependence of T_1 shortening. Signal intensity resulting from proton spin realignment to the main magnetic field after excitation from repetitive RF pulses was measured. The signal received is dependent on T_1 and the repetition times (TR) between RF pulses. The dependency of signal on TR is illustrated in Fig. 1a for an $MnSO_4$ liposome-DOX formulation measured over a range of drug concentrations (T = 29.9°C). The data were fit to Eq. 1 to obtain relative proton density

(PD), spin-lattice relaxation time constant (T_1), and baseline noise (C) for each concentration/temperature combination:

$$Signal = PD(1 - \exp(-TR/T_1)) + C. \quad [1]$$

The rate of rise of signal vs. TR increases with Mn^{2+} and drug concentration, due to T_1 shortening (Fig. 1a). Changes in the asymptotic value of each curve, PD, are governed by the number of protons in each sample and by the effects of T_2. There is a linear relationship between the reciprocal of T_1 ($1/T_1$) and the $MnSO_4$ concentration. The slope of this line is the "relaxivity" $(mM*sec)^{-1}$ (6) (Fig. 1b).

Relaxivity changed as a function of temperature, but this relationship was quite different for free $MnSO_4$ ± DOX and the NTSL (Fig. 1c). $MnSO_4$ + empty LTSL and free $MnSO_4$ ± DOX exhibited decreased relaxivity with increased temperature, presumably due to increased thermal motion of H_2O and Mn, which limits the interaction of Mn^{2+} with H_2O (5,7). $MnSO_4$ + DOX and $MnSO_4$ – DOX had identical relaxivity profiles, indicating that DOX, at a concentration expected to be seen in vivo, has no effect on relaxivity of $MnSO_4$ in solution. In contrast, relaxivity of NTSL ± DOX increased as temperature was raised. At elevated temperatures, permeability of the liposome bilayer increases to both water and Mn^{2+}. It is known that water permeability is much greater than that observed for ions; thus, we anticipate that water exchange will be much faster than Mn^{2+}. The inverted temperature dependence is therefore probably due an increase in water exchange across the lipid bilayer (16,27). The relaxivity measurements were taken at sequentially increasing followed by decreasing temperatures, and there was no hysteresis seen indicating that Mn^{2+} remained encapsulated.

Linear regressions for relaxivity as a function of temperature were obtained for all in vitro samples (Fig. 1c). $MnSO_4$ + LTSL, $MnSO_4$, and NTSL ± DOX had slopes ± SE of −0.166 ± 0.023, −0.082 ± 0.003, and 0.064 ± 0.005 $(mM*sec*°C)^{-1}$ and intercepts ± SE of 13.67 ± 0.087, 7.28 ± 0.12, and −1.41+0.18 $(mM*sec)^{-1}$, respectively. These results are similar to previous results reported for free $MnCl_2$ and comparable to other liposome formulations using Gd loaded into liposomes and/or surface-bound (10–12,27). For comparison, Gd-DTPA (Magnevist) has a relaxivity of ~4–4.5 $(mM*sec*°C)^{-1}$ (13) at physiological temperatures.

Relaxivity measurements for LTSL showed a complex temperature relationship (Fig. 1d). The measurements were taken below and above the gel to liquid phase transition temperature for this formulation (39.5–40°C) (20). Measurements started below the transition temperature, raised beyond the transition, and then as the solutions were cooled below the transition (see arrows, Fig. 1d). During the initial heating period, LTSL had relaxivity values similar to those of the NTSL. When the phase transition temperature for LTSL was approached, however, relaxivity dramatically increased to levels nearly equivalent to those for free $MnSO_4$ + empty LTSL. This was expected as content release from the LTSL occurs within seconds of reaching the transition temperature (20). Once liposomal contents were released, further heating showed decreased relaxivity, consistent with behavior of free $MnSO_4$ in solution. Relaxivity increased during subsequent cooling in a manner parallel to $MnSO_4$ + empty LTSL. The relaxivity of $MnSO_4$ loaded LTSL, postrelease, was −0.157 ± 0.017 $(mM*sec*°C)^{-1}$, which is the same as that of $MnSO_4$ + empty LTSL at −0.166 ± 0.023 $(mM*sec*°C)^{-1}$. However, the intercepts for LTSL and the $MnSO_4$ + empty LTSL are somewhat different, suggesting that the liposomes did not release all of their contents, as reported previously (20).

Characterization of Temperature Distribution From Local Hyperthermia Device

The MRI-compatible heating device (Fig. 2a) yielded a radially oriented thermal profile in vivo, which was hottest near the catheter wall and decreased radially toward the tumor periphery (Fig. 2b). The data were fit to the radial 1D steady-state heat transfer equation in Eq. 2, which is governed by the thermal conductivity of the tissue (k) and its internal heat generation (Q):

$$T(r) = \frac{Q}{4k} r^2 + C_1 \ln(r) + C_2. \quad [2]$$

The temperature profile data were fit using nonlinear regression yielding 0.0202 ± 0.0034°C/mm^2, −3.464 ± 0.1397°C/ln(mm), and 43.574 ± 0.1357°C for Q/4k, C_1, and C_2, respectively.

In the imaging experiments, the bore of the magnet had an elevated ambient air temperature of 36–39°C, while in the laboratory the temperature is typically 21–23°C. The elevated ambient air temperature maintained the animal's body temperature in the MRI, using a feedback hot air system (24). The increased air temperature reduced heat loss, affecting the thermal boundary conditions on the tumor. This resulted in a different thermal profile than the one measured in the laboratory. Because of the space limitations and the presence of the magnetic field in the MRI device, it was not possible to completely measure the thermal profile with a micromanipulator.

However, some manual measurements were made in the MRI. These measurements were combined with those made in the laboratory to estimate the temperature distribution of the tissue when placed in the magnet. Thermocouple measurements were made at: 1) the intradermal surface of the tumor, 2) the heating catheter surface, 3) the tumor tissue 2.5–3 mm from the catheter, 4) muscle underlying the tumor, and 5) the heated air stream. Tumor temperatures ranged from 44–39.5°C (catheter and skin, respectively; Fig. 2d).

The thermal profile within the bore of the magnet was calculated using data from Fig. 2b and Eq. 2. The thermal properties of the tumor (k and Q) were derived from room air measurements and were assumed to remain constant between the two heating environments. Using Eq. 2, the integration constants C1 and C2 were calculated with the data from the boundary condition measurements taken when the animals were in the MRI device (Fig. 2c).

The predicted thermal profile (Fig. 2d) in the MRI shows good agreement with the independent measurements taken for this configuration that were not used for the simulation (Fig. 2d). The predicted thermal data are highly

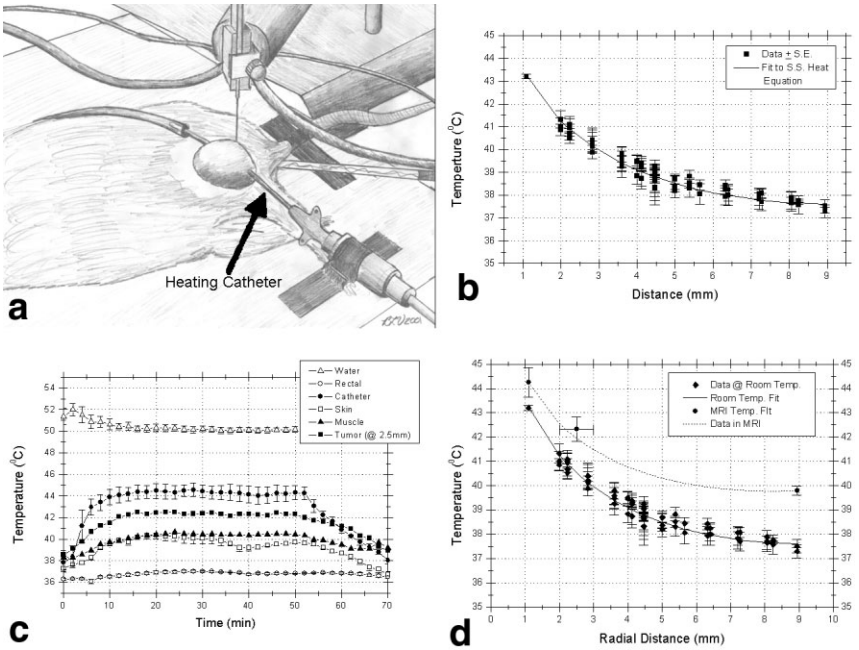

FIG. 2. **a:** Cartoon of MRI compatible local hyperthermia device. **b:** Radial temperature measurements (■) of four animals. (—) Nonlinear regression fit using the steady state 1D radial heat transfer equation. **c:** Temperature profile within the MRI of (△) heating water within the catheter, (○) rectal temperature of the rat, (●) surface temperature of the catheter (tumor side), (□) tumor surface temperature at the skin, (▲) muscle temperature (underneath the tumor), and (■) tumor (2.5 mm from the catheter). **d:** Nonlinear regression fit for the temperate profile in the MRI (----) using the boundary conditions from **c** and the physical properties obtained from **b**. (—) Nonlinear regression fit using the steady state 1D radial heat transfer equation.

relevant to the MR results, as described below. Importantly: 1) Local HT treatment of the tumor was achieved, while maintaining a constant rectal temperature that was below the transition temperature of the LTSL (Fig. 2c); 2) The temperature at the periphery of the tumor was estimated to be ≥39.5°C, which is near the transition temperature of the LTSL; 3) Steady state heating was reached after 15–20 min (Fig. 2c), indicating that at the time of liposome injection temperatures were stable.

In Vivo Imaging

Sixteen slice (12 useable) 3D volume images were obtained at an in-plane resolution of 234 × 234 μm and a slice thickness of 1.3 mm. Comparison of LTSL + HT, LTSL alone, NTSL + HT, and NTSL alone from 0–90 min is shown in Fig. 3. In the first row of Fig. 3 the tumor margin is labeled along with the heating catheter, vessels, and unheated muscle. For LTSL + HT, rapid signal enhancement occurred at the tumor periphery, which remained elevated until the end of the experiment. LTSL alone showed relatively homogenous signal enhancement that peaked at 5 min and then began to decline. NTSL + HT showed heterogeneous signal enhancement that increased throughout the experiment. NTSL alone showed marginal, but detectable, enhancement in the tumor and normal tissue at 5 min postinjection. All other time points were equivalent to background.

Quantitative Image Analysis

Signal Intensity Ratio (SIR)

Four ROIs were selected for image analysis: a tumor-enhancing region (TE), a tumor-nonenhancing region (TN), unheated muscle, and vessel. The signal intensities of the ROIs and vessel were measured for each slice. An example of these data is shown in Fig. 4a. Signal intensity data were normalized to the muscle signal to yield SIR.

Vessel SIR for LTSL ± HT rapidly increased after liposome injection, reaching a peak at 2.5 at 3–4 min (Fig. 4b). SIR then began to decrease, reflecting clearance of liposomes from the vasculature. TE regions showed immediate and substantial increases in SIR values that were equivalent to vessel SIR values. These values remained elevated at 2.25 after 15–20 min (Fig. 4b). In contrast to the TE region, the TN region showed slow increase in SIR, rising from 0.75 at 3 min to 1.1 after 60 min of heating (Fig. 4b). The slow increase in TN regions suggests that free Mn was diffusing into this region from the surrounding TE regions. The initial drop in the SIR in the TN regions was caused by the brief initial rise in muscle signal shortly after LTSL injection, which reflected the presence of circulating liposomes.

The vessel SIR of LTSL alone reached a peak value of 2.5 at 3 min (Fig. 4c), similar to the SIR in the LTSL+ HT case (Fig. 4b). The vessel SIR decreased after reaching the peak, but did not return to a value of 1 by the end of 60 min, suggesting that the LTSL circulate longer without HT than with HT (Fig. 4c). The TE region increased from a baseline of 0.75 to a peak of 1.25 by 6 min (Fig. 4c). The SIR then slowly decreased and plateaued at a value of 1.1. The initial increase in SIR probably reflects delivery of liposomes to the tumor via perfusion. The sustained elevated value is evidence of liposomal accumulation in the tumor due to extravasation. TN regions were not found in the LTSL alone group (Fig. 3).

The vessel SIR of NTSL alone reached peak values of 2.75–3.0 at 5 min (Fig. 4d), similar to the LTSL+HT and NTSL+HT cases (Fig. 4b,c). SIR also decreased after reaching the peak, but did not return to a value of 1 during the heating procedure (Fig. 4d). The TE region increased from a baseline of 0.75 throughout the experiment to a value of 1.4 by 60 min (Fig. 4d). This continuous rise in SIR probably reflects liposome extravasation. TN regions of the tumor remains fairly constant, with a slight rise 5 min

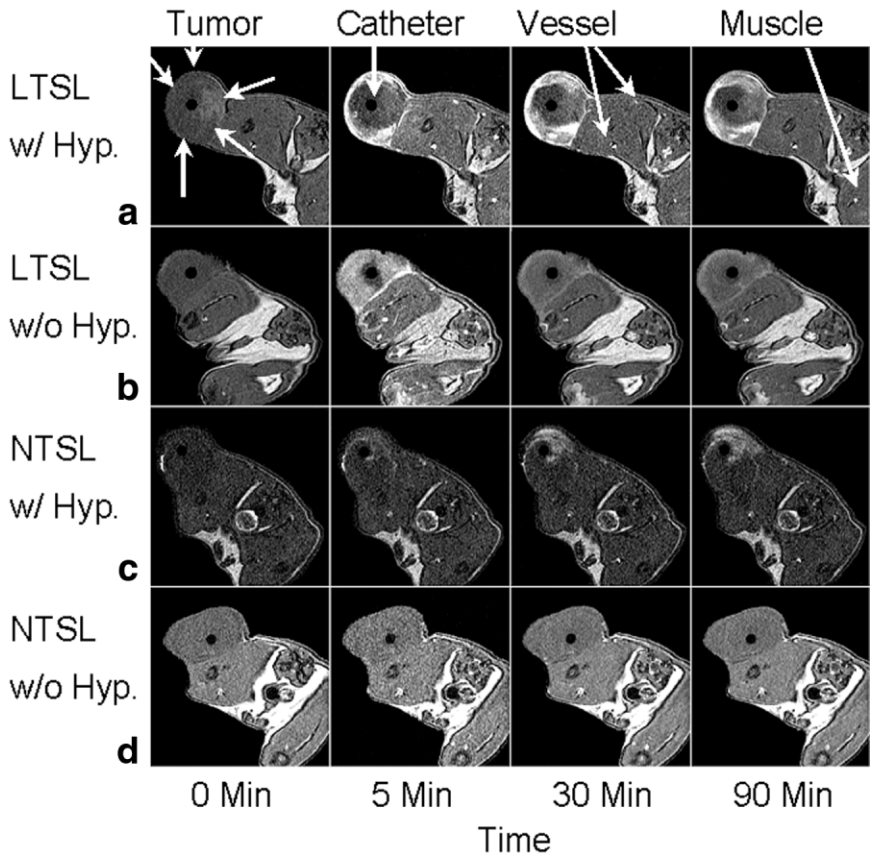

FIG. 3. MRI axial image results of rats with transplanted flank fibrosarcomas treated with (**a**) LTSL with HT, (**b**) LTSL without HT, (**c**) NTSL with HT, and (**d**) NTSL without HT from 0–90 min. **a:** The LTSL with HT (slice 5 from Fig. 4) shows rapid signal enhancement that remains through the experiment at the periphery of the tumor. This enhancement is heterogeneous but localized only with in the tumor. **b:** LTSL without HT shows less intense but more uniform signal enhancement in tumor. That peaks at 5 min and then fades as clearance of LTSL from the vasculature occurs. **c:** NTSL with HT has an intermediate result between the LTSL with and without HT. There is heterogeneous distribution of the NTSL as with the LTSL with HT (**a**), but the distribution penetrates to the catheter. **d:** The NTSL without HT shows minimal enhancement at 5 min, which reflects the presence of liposomes in the vasculature. The flank tumor is indicated along with the heating catheter, venous vessels, and unheated muscle

postinjection. This rise is not significant, but does correspond to the peak SIR seen in the vessels.

Radial Signal Distribution Method

This method was devised to facilitate comparison of the signal enhancement data with the radial temperature distribution during heating. An example of this method is shown for one LTSL + HT experiment. RSD was calculated for LTSL with HT from Fig. 3 (Fig. 5a–c). RSD was constant across the tumor at time = 0 (Fig. 5a). At 5 min postinjection (Fig. 5b), the RSD showed significant signal increase at the tumor periphery. At 60 min RSD was still elevated at the tumor periphery but the intensity elevation broadened inward toward the center of the tumor (Fig. 5c).

From the results shown in Fig. 3d, the temperature at the periphery of the tumor is ~39.5°C, which is in the range of the transition temperature for this liposome (20). The in vitro data from this study verifies that the transition temperature is in this range (Fig. 2d). Consequently, content release from the liposome is the most likely explanation for the increase in signal intensity at this location. We can rule out the possibility that the increase in RSD was due to elevated temperature because the signal intensity remained elevated even after the temperature of the tumor was allowed to return to baseline (data not shown).

DISCUSSION

The results of this study are highly relevant for the development of methods to optimize and monitor liposomal drug delivery and content release. The ability to obtain serial measurements noninvasively will allow determination of tissue pharmacokinetics and assessment of intratumoral heterogeneity with respect to drug delivery.

The in vitro results illustrate that these liposome formulations are imageable in their intact form and that content release can be observed in LTSLs upon heating. The hysteresis observed in relaxivity when the LTSLs were heated and then cooled below their transition temperature serves as confirmation of content release.

It is known that these liposomes do not release all of their contents, which is probably the reason the LTSL + Mn^{2+} have a higher relaxivity than Mn^{2+} loaded liposomes that were heated to release their contents (20). Additionally, the results suggest that there is an interaction between the Mn^{2+} and the LTSL upon heating. This interaction is seen in comparing the increased relaxivity of Mn^{2+} and LTSL above free Mn^{2+}. Although the nature of the interaction is unknown, it could be due to partial binding of the Mn^{2+} cation with the phospholipid head groups on the liposomes serving as the anion. This coordination would reduce the Brownian motion of Mn^{2+}, thereby increasing its interaction with water. This would raise the relaxivity (5).

The results of the study show that the liposomes are imageable within the drug dose used (10 mg/kg) for therapy. Although drug release was not measured directly in this study, it has been shown that DOX encapsulated in this liposome formulation with a pH gradient loading method is released when the transition temperature of the

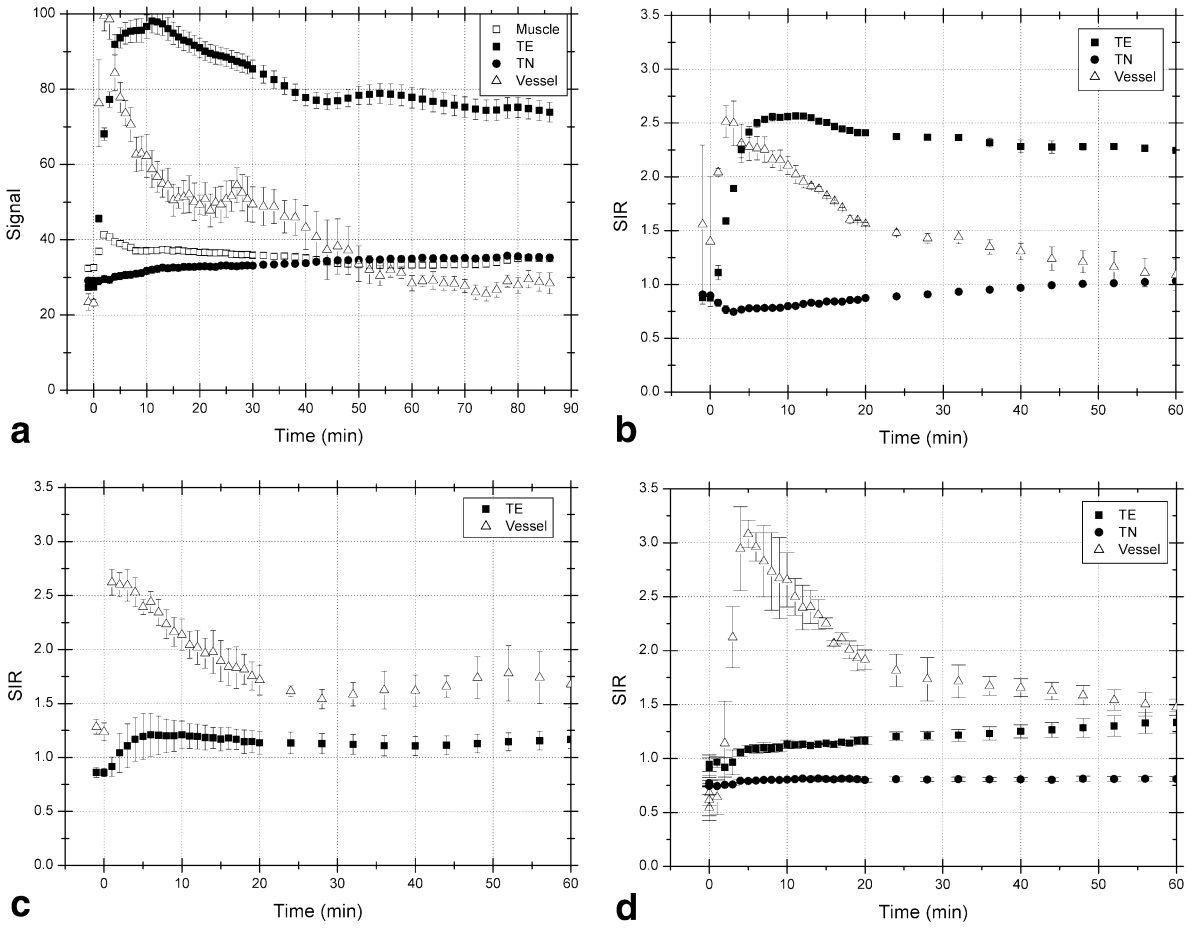

FIG. 4. **a:** Signal intensity as a function of time of LTSL with HT from Fig. 3. Signal for the (□) muscle, (■) tumor-enhancing region (TE), (●) tumor nonenhancing region (TN), and (△) vessel are shown. **b:** Signal intensity ratio (SIR) for LTSL with HT for the (■) TE, (●) TN, and (△) vessel. There is rapid increase in both the vessel and TE SIR. However, the TE SIR remains elevated though the experiment, indicating that accumulation and/or content release is occurring at the tumor site. Signal enhancement remained after cooling (see text). The vessel SIR decreases after reaching a maximal value 3 min postinjection. The TN region shows minimal increase in SIR through the course of the experiment. This could be caused by diffusion of liposome contents from the area of high concentration to the TN region. **c:** SIR values for the LTSL without HT for the (■) TE and the (△) vessel region are shown. The vessel SIR increases in the same manner as the LTSL with HT experiments. SIR of the TE region increases over the same time frame as the LTSL + HT. The ratio remains relatively low, compared with LTSL + HT, but it does not return to baseline by 60 min. This indicates that accumulation of liposomes is occurring. **d:** SIR values for the NTSL with HT for the (●) tumor nonenhancing region (TN), (■) tumor enhancing region TE, and the (△) vessel region are shown. Vessel SIR increases in the same manner as the LTSL with HT and LTSL without HT experiments. SIR of the TE region increases over the experiments, indicating liposome extravasation. The TN region does not enhance. Signal intensity was averaged over 12 slices (error bars in **a**). SIR was calculated using the ratio of these averages. The data plotted were obtained by averaging SIRs obtained from three animals (error bars in **b,c,** and **d**).

liposome is reached (4,20). In addition, we verified that temperature-dependent drug release occurs from this formulation in independent in vitro experiments (data not shown) (4,20). Additional studies are ongoing to compare Mn^{2+} MR signal distribution to drug concentration. This is the foundation for a second article.

In vivo release of contents was also seen in response to local hyperthermia. This conclusion is based on four observations: 1) A unique pattern of peripheral MR signal enhancement seen in LTSL + HT experiments that was absent from the other three groups; 2) dynamic contrast imaging with Gd-DTPA showed that the perfusion pattern flows from the periphery to the center (data not shown); 3) the temperature at the periphery of the tumor is at the transition temperature for the liposome (20); and 4) the enhancement in the tumor periphery remained after heating was discontinued, indicating that HT did not cause hysteresis effects that would confound interpretation of the results.

The lack of signal enhancement in the center of the tumor is not likely due to central necrosis or damage from the heating catheter. Our experiments with LTSL alone and NTSL + HT have shown that the heating catheter and local HT do not adversely affect the perfusion of the FSA tumor, respectively, since we see signal enhancement next to the catheter in these cases. Additionally, relatively homogenous vascular density has been observed in this tumor type and H&E staining of these tumors after treatment

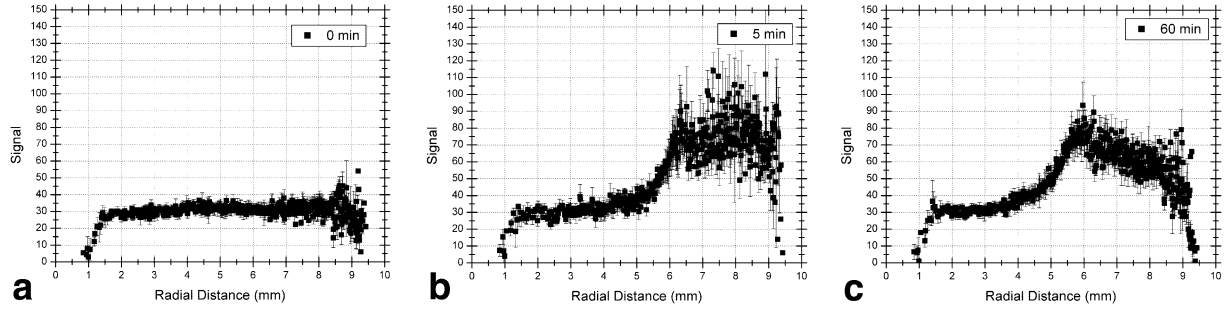

FIG. 5. **a:** RSD analysis for LTSL with HT, slice 5 from Fig. 4/5 is shown at *t* equals 0 min. **b,c:** RSD analysis for 5- and 60-min time points, respectively. From **a** the signal is constant through out the radius of the tumor. Five minutes after liposome injection (**b**) there is significant signal enhancement seen at the periphery of the tumor (also seen in Fig. 4/5). This signal enhancement is present at 60 min postinjection (**c**), but the signal enhancement begins to progress toward the center of the tumor.

indicates lack of central necrosis (Fig. 6). The implications of the enhancement pattern seen in the LTSL + HT is that homogenous drug delivery might be difficult, since the kinetics of liposomal content release is significantly shorter then the liposomal circulation time within the tumor (20). Consequently, the liposomes have their contents depleted by the time they reach the center. This release pattern might be used in an advantageous manner, targeting the periphery of the tumor where the neovascularization is present if the liposomes are loaded with vascular targeting agents.

This imaging method can also be used to monitor liposome accumulation in tumors outside the RES. Liposome extravasation is known to occur in tumors as a result of large endothelial gaps (1,28). This lack of vascular integrity is believed to be due to the immature nature of the tumor microcirculation (1). This property is one of the major methods used to target liposomal directed therapy (1,17,19), and is shown here with the increase in SIR of LTSL in the absence of HT. The fact that SIR does not return to baseline at the end of these experiments is evidence that liposomal extravasation and retention must have occurred in the tumor.

FIG. 6. Typical H&E staining of a cryosection of tumor excised at the end of an imaging experiment. There is no necrosis in the section, further supporting the conclusion that the peripheral distribution of signal enhancement in the LTSL + HT group is due to enhanced drug release from the liposomes, as opposed to decreased vascularity, as might occur iatrogenically from the presence of the catheter.

HT is known to increase endothelial gap sizes of tumor microvessels, improving liposome accumulation (1,17,19). The HT device used for this study provided a reproducible thermal profile that was well characterized, yielding local HT in the temperature range needed to increase extravasation (1,17,19) and content release (20). The effect of improved extravasation and accumulation with HT is shown in the NTSL + HT experiments compared to NTSL alone. In the former case signal remained elevated after 60 min, whereas persistent signal enhancement was not seen with NTSL alone.

Several methods have previously been used to image liposomal drug delivery (2,8,9,11,12,14–16,27,29,30). Successful imaging of liposomal drug delivery should yield data with the following characteristics: 1) high signal-to-noise ratio (S/N) at pharmacologically relevant concentrations; 2) a signal-based parameter that can be related to drug concentration; and 3) high spatial and temporal resolution. Finally, the ideal agent for clinical application would also be one that provides imaging and therapy in the same vehicle.

PET has excellent sensitivity for detection of radiolabeled compounds and tracer amounts of radiolabeled substances can be administered to obtain quantitative data (8). However, spatial resolution is significantly sacrificed compared to other methods. CT imaging provides excellent spatial resolution but requires a contrast agent (i.e., iodine) that can be loaded into liposomes (2). Also temporal resolutions may be inferior to PET or MRI, where multiple images/min are easily acquired (2). A limitation to both PET and CT is that they cannot provide signal that reflects physical changes in the condition of the drug carrying liposome, such as would occur when contents are released.

Our formulated liposomes and choice of imaging modality (MRI) provides solutions to these problems: 1) The imaging agent (Mn) is inherent to the drug loading method for this liposome and the signal obtained is dependent on whether it is encapsulated or in free solution; 2) The liposomes provide reasonable MR S/N at pharmacologi-

cally relevant concentrations (18); and 3) Good temporal resolution can be obtained.

Suitability as a dual MR contrast and drug delivery agent also requires that the contrast agent be nontoxic systemically with respect to the cytotoxic drug as well as the Mn^{2+} that will be released. The imaging was conducted using the maximally tolerated liposomal DOX dose of 10 mg/kg, which fulfills the first criterion. The corresponding Mn dose is 78.3 μmol/kg, which is 30% of the single dose LD_{50} of Mn^{2+} (272 μmol/kg) (10). Thus, it is unlikely that Mn^{2+} will be toxic, but additional studies need to be done to clarify this point. Alternatively, one could use other divalent paramagnetic cations that are less toxic as drug loading agents.

This imaging technique could also be applied to the evaluation of liposomal formulations that release contents under other types of triggers, such as pH (31). This ability to monitor liposomal/drug delivery and/or content release in real time could allow for development of treatment strategies to improve intratumoral homogeneity of drug concentration.

REFERENCES

1. Kong G, Dewhirst MW. Hyperthermia and liposomes. Int J Hyperthermia 1999;15:345–370.
2. Bhatnagar A, Hustinx R, Alavi A. Nuclear imaging methods for noninvasive drug monitoring. Adv Drug Deliv Rev 2000;41:41–54.
3. Holland JF, Frei E (eds.). Cancer Medicine 6th ed, vol. 1-2. Hamilton, Ontario: BC Decker; 2003.
4. Abraham S, Edwards K, Karlsson G, MacIntosh S, Mayer L, McKenzie C, Bally M. Formation of transition metal-doxorubicin complexes inside liposomes. Biochim Biophys Acta 2002;1565:41.
5. Wehrli FW, Shaw D, Kneeland JB. Biomedical magnetic resonance imaging: principles, methodology, and applications. New York: Virchow; 1988.
6. Morgan L, Nolle A. Proton spin relation in aqueous solutions of paramagnetic ions II: Cr+++, Mn++. Ni++, Cu++, and Gd++. J Chem Phys 1959;31:365.
7. Liang Z-P, Lauterbur PC. Principles of magnetic resonance imaging: a signal processing perspective. New York: SPIE Optical Engineering Press; IEEE Press; 2000.
8. Matteucci ML, Anyarambhatla G, Rosner G, Azuma C, Fisher PE, Dewhirst MW, Needham D, Thrall DE. Hyperthermia increases accumulation of technetium-99m-labeled liposomes in feline sarcomas. Clin Cancer Res 2000;6:3748–3755.
9. Leander P, Mansson S, Ege T, Besjakov J. CT and MR imaging of the liver using liver-specific contrast media. A comparative study in a tumour model. Acta Radiol 1996;37:242–249.
10. Niesman MR, Bacic GG, Wright SM, Swartz HJ, Magin RL. Liposome encapsulated MnCl2 as a liver specific contrast agent for magnetic resonance imaging. Invest Radiol 1990;25:545–551.
11. Schwendener RA, Wuthrich R, Duewell S, Wehrli E, von Schulthess GK. A pharmacokinetic and MRI study of unilamellar gadolinium-, manganese-, and iron-DTPA-stearate liposomes as organ-specific contrast agents. Invest Radiol 1990;25:922–932.
12. Suga K, M MP, Ogasawara N, Okazaki H, Matsunaga N. Potential of Gd-DTPA-mannan liposome particles as a pulmonary perfusion MRI contrast agent: an initial animal study. Invest Radiol 2001;36:136–145.
13. Unger E, Fritz T, Shen DK, Wu G. Manganese-based liposomes. Comparative approaches. Invest Radiol 1993;28:933–938.
14. Chu WJ, Simor T, Elgavish GA. In vivo characterization of Gd(BME-DTTA), a myocardial MRI contrast agent: tissue distribution of its MRI intensity enhancement, and its effect on heart function. NMR Biomed 1997;10:87–92.
15. Unger E, Shen DK, Wu GL, Fritz T. Liposomes as MR contrast agents: pros and cons. Magn Reson Med 1991;22:304–308; discussion 313.
16. Bacic G, Niesman MR, Bennett HF, Magin RL, Swartz HM. Modulation of water proton relaxation rates by liposomes containing paramagnetic materials. Magn Reson Med 1988;6:445–458.
17. Kong G, Braun RD, Dewhirst MW. Characterization of the effect of hyperthermia on nanoparticle extravasation from tumor vasculature. Cancer Res 2001;61:3027–3032.
18. Kong G, Anyarambhatla G, Petros WP, Braun RD, Colvin OM, Needham D, Dewhirst MW. Efficacy of liposomes and hyperthermia in a human tumor xenograft model: importance of triggered drug release. Cancer Res 2000;60:6950–6957.
19. Kong G, Braun RD, Dewhirst MW. Hyperthermia enables tumor-specific nanoparticle delivery: effect of particle size. Cancer Res 2000;60:4440–4445.
20. Needham D, Anyarambhatla G, Kong G, Dewhirst MW. A new temperature-sensitive liposome for use with mild hyperthermia: characterization and testing in a human tumor xenograft model. Cancer Res 2000;60:1197–1201.
21. Cheung BC, Sun TH, Leenhouts JM, Cullis PR. Loading of doxorubicin into liposomes by forming Mn2+-drug complexes. Biochim Biophys Acta 1998;1414:205–216.
22. Mayer LD, Hope MJ, Cullis PR, Janoff AS. Solute distributions and trapping efficiencies observed in freeze-thawed multilamellar vesicles. Biochim Biophys Acta 1985;817:193–196.
23. Fiske CH, Subbarow Y. The colour/metric determination of phosphorus. J Biol Chem 2 1925:375–395.
24. Qiu H, Cofer G, Hedlund L, Johnson GA. Automated feedback control of body temperature for small animal studies with MR microscopy. IEEE Trans Biomed Eng 1997;44:1107–1113.
25. Grant JP, Wells SA Jr. Tumor resistance in rats immunized to fetal tissues. J Surg Res 1974;16:533–540.
26. Takehara Y, Sakahara H, Masunaga H, Isogai S, Kodaira N, Takeda H, Saga T, Nakajima S, Sakata I. Tumour enhancement with newly developed Mn-metalloporphyrin (HOP-9P) in magnetic resonance imaging of mice. Br J Cancer 2001;84:1681–1685.
27. Fossheim SL, Fahlvik AK, Klaveness J, Muller RN. Paramagnetic liposomes as MRI contrast agents: influence of liposomal physicochemical properties on the in vitro relaxivity. Magn Reson Imag 1999;17:83–89.
28. Yuan F, Dellian M, Fukumura D, Leunig M, Berk DA, Torchilin VP, Jain RK. Vascular permeability in a human tumor xenograft: molecular size dependence and cutoff size. Cancer Res 1995;55:3752–3756.
29. Unger EC, Shen DK, Fritz TA. Status of liposomes as MR contrast agents. J Magn Reson Imag 1993;3:195–198.
30. Bulte JW, de Cuyper M, Despres D, Frank JA. Short- vs. long-circulating magnetoliposomes as bone marrow-seeking MR contrast agents. J Magn Reson Imag 1999;9:329–335.
31. Lokling KE, Skurtveit R, Fossheim SL, Smistad G, Henriksen I, Klaveness J. pH-sensitive paramagnetic liposomes for MRI: assessment of stability in blood. Magn Reson Imag 2003;21:531–540.